Trajectory Tracking for Marine Vehicles under Constant Disturbances: Controller Design and Tuning

M. Burger and K.Y. Pettersen
Norwegian University of Science and Technology (NTNU),
Department of Engineering Cybernetics, NO-7491, Trondheim, Norway.
Email: Mernout.Burger@itk.ntnu.no

***Abstract*—This article discusses target tracking for marine vehicles in the presence of constant disturbances. In previous work the stability analysis for the system has been discussed. In this article we show both theoretically and by simulation what the effect of the tuning parameters on the closed-loop system is, and provide a set of tuning rules.**

I. Introduction

For exploring the oceans—either for research, harvesting resources or defence purposes—the use of unmanned vehicles is increasing. Whether the vessel is an autonomous surface vehicle (ASV) or an autonomous underwater vehicle (AUV), it can be subjected to external disturbances. In this paper we focus on the influence of constant external disturbances affecting surface vessels, such as wind and ocean currents.

If ocean currents are not taken into account in the controller, the marine vehicles will either drift away, or follow the path at a distance from the desired path. For operations where the position of the vessel is important the vessel should be able to follow its desired path closely—despite the disturbance of the unknown ocean currents—in order to obtain accurate measurement data, or be at the right place at the right time.

This article is based on the work done in [1], [2], in which the stability of the system is discussed and proven. In this article we generalise this work slightly by using tuning matrices instead of scalars, and we focus on the applicability of the controller, by supporting our claim of easy tunability through explaining the effect of the different tuning parameters.

In Section II we discuss the vessel model and the proposed controller. A conditional integrator is used to cope with external disturbances, and the properties of it are given in Section III. The the tuning of the system is discussed based on both the expected theoretical effect on the error dynamics given in Section IV, and the graphical results of simulations in Section IV. Conclusions are drawn in Section V.

II. Vessel Model and Controller Design

We use **conditional integrators** (CIs), which is a control method recently proposed in [3], [4], inheriting the benefits of proportional-integral (PI) control and sliding mode control, while avoiding the disadvantages of the two methods. For large errors, CIs behave like sliding mode controllers, thereby providing a *bounded control effort* and providing *integrator anti-windup*. For small errors, CIs behave like PI controllers, resulting in *smooth control signals* with *clear tuning rules*. The *robustness against disturbances* is inherited from both methods. These good properties make it an attractive control method for autonomous marine vehicles, which have limited battery capacity and are subjected to unknown currents.

We consider the 3 degrees-of-freedom (DOF) surface vessel model of the form ([5]):

$$\dot{\eta} = \mathbf{J}(\eta)\nu \tag{1}$$

$$\mathbf{M}\dot{\nu} + \mathbf{C}(\nu)\nu + \mathbf{D}(\nu)\nu + \mathbf{J}^{\top}(\eta)\epsilon = \tau, \tag{2}$$

where $\eta = [x,\, y,\, \psi]^{\top}$ contains the position coordinates x and y, and orientation angle ψ of the vessel in an inertial reference frame. The vector $\nu = [u,\, v,\, r]^{\top}$ contains the linear velocities u (surge) and v (sway), and the angular velocity r (yaw rate) in the body-fixed reference frame; τ is the control input of the system, and ϵ represents a disturbance constant in the inertial frame. $\mathbf{M} = \mathbf{M}^{\top} \succ \mathbf{0}$ represents the mass matrix, $\mathbf{C}(\nu) = -\mathbf{C}^{\top}(\nu)$ is the Coriolis and centripetal matrix and $\mathbf{D}(\nu) \succ \mathbf{0}$ is the damping matrix. The matrix $\mathbf{J}(\eta)$ satisfies

$$\mathbf{J}^{\top}(\eta)\mathbf{J}(\eta) = \mathbf{J}^{-1}(\eta)\mathbf{J}(\eta) = \mathrm{I}, \quad \|\mathbf{J}(\eta)\| = 1. \tag{3}$$

where $\|\cdot\|$ denotes the 2-norm $\|\cdot\|_2$. For ease of notation, we often write $\mathbf{C}$, $\mathbf{D}$ and $\mathbf{J}$ instead of $\mathbf{C}(\nu)$, $\mathbf{D}(\nu)$ and $\mathbf{J}(\eta)$.

The *desired pose* $\eta_{\mathrm{d}}(t)$ gives the desired position and orientation on the path at time instant t. For the body-fixed velocities in ν, we consider two distinct notions of 'desirable' values. We define the *desired velocity* ν_{d} as the velocity of the target on the path, given by

$$\nu_{\mathrm{d}} := \mathbf{J}^{\top}(\eta_{\mathrm{d}})\dot{\eta}_{\mathrm{d}}, \tag{4}$$

which is dependent on the path and on time. In order to obtain convergence to the path, we use the tuning parameter $\mathbf{E} \succ \mathbf{0}$ and define the *commanded velocity* ν_{c} as

$$\nu_{\mathrm{c}} := \mathbf{J}^{\top}(\eta)\left[\dot{\eta}_{\mathrm{d}} + \mathbf{E}\tilde{\eta}\right] \tag{5}$$

which is dependent on the path, time, and the current state. The vessel should track the commanded velocity ν_{c}, which in turn should guarantee convergence towards the desired velocity ν_{d}. The state error vectors are defined as

$$\tilde{\eta} := \eta_{\mathrm{d}} - \eta, \qquad \tilde{\nu} := \nu_{\mathrm{c}} - \nu. \tag{6}$$

We propose the use of an inner feedback control law

$$\tau = \mathbf{M}\dot{\nu}_{\mathrm{c}} + \mathbf{C}(\nu)\nu_{\mathrm{c}} + \mathbf{D}(\nu)\nu_{\mathrm{c}} - \bar{\tau}, \tag{7}$$

978-1-4244-5222-4/10/$26.00 ©2010 IEEE

where the auxiliary control vector $\bar{\tau}$ is chosen as

$$\bar{\tau} = -\mathbf{F}\mathbf{sat}\left(\mathbf{H}^{-1}\left[\tilde{\nu} + \mathbf{J}^{\top}\mathbf{G}\sigma\right]\right) \tag{8a}$$
$$\dot{\sigma} = -\mathbf{G}\sigma + \mathbf{J}\mathbf{H}\mathbf{sat}\left(\mathbf{H}^{-1}\left[\tilde{\nu} + \mathbf{J}^{\top}\mathbf{G}\sigma\right]\right) \tag{8b}$$

where the tuning parameters $\mathbf{F} \succ \|\epsilon\|\,\mathrm{I}$, $\mathbf{G} \succ \mathbf{0}$, $\mathbf{H} \succ \mathbf{0}$ are diagonal matrices commuting with $\mathbf{J}$ (e.g. $\mathbf{FJ} = \mathbf{JF}$), and $\mathbf{sat}(\cdot)$ is an element-wise saturation function, given by

$$\mathbf{sat}(s) = \begin{bmatrix} \mathrm{sat}(s_1) \\ \vdots \\ \mathrm{sat}(s_n) \end{bmatrix}, \quad \mathrm{sat}(s_i) = \begin{cases} -1 & : \quad s_i < -1 \\ s_i & : \quad |s_i| \leq +1 \\ +1 & : \quad s_i > +1 \end{cases} \tag{9}$$

for some vector $\mathbf{s} \in \mathbb{R}^n$, where s_i denotes the i-th element of the vector $\mathbf{s}$.

In [2] it is shown that for $\{\mathbf{E},\, \mathbf{F},\, \mathbf{G},\, \mathbf{H}\} = \{\alpha\mathrm{I},\, \kappa\mathrm{I},\, \gamma\mathrm{I},\, \mu\mathrm{I}\}$ the system is uniformly globally asymptotically stable and uniformly locally exponentially stable. Using the same methods, it can be proven that if $\mathbf{F}$ and $\mathbf{H}$ are chosen such that $\mathbf{FJ} = \mathbf{JF}$ and $\mathbf{F} = c\mathbf{H}^{-1}$ for some scalar $c > 0$, these stability properties are preserved (see [6]). Using the auxiliary state vector σ, we can obtain an estimate of the disturbance ϵ as

$$\hat{\epsilon} := \mathbf{K}_{\epsilon}^{-1}\sigma, \qquad \mathbf{K}_{\epsilon} := \mathbf{F}^{-1}\mathbf{G}^{-1}\mathbf{H} \succ \mathbf{0}. \tag{10}$$

III. Properties of the Conditional Integrator

The conditional integrator as given in (8) has some desirable properties, which will be discussed in this section. For ease of notation we introduce the vector

$$\mathbf{s} := \mathbf{H}^{-1}\left[\tilde{\nu} + \mathbf{J}^{\top}\mathbf{G}\sigma\right], \tag{11}$$

which can be seen as the *sliding surface* as used in sliding-mode control in case the saturation function in (8) is saturated (in which case it behaves like a sign function).

A. Bounded and smooth control signal

As can be seen from (8a), the control signal $\bar{\tau}$ is bounded in amplitude; the elements of the saturation function always have values between -1 and 1, and hence the amplitude of the i-th element $\bar{\tau}_i$ of $\bar{\tau}$ is given by f_i, which denotes the i-th element on the diagonal of $\mathbf{F}$. Due to the use of a saturation function rather than a sign function, the signal $\bar{\tau}$ remains smooth, and does not introduce chattering in the system.

B. Integrator anti-windup

The auxiliary state vector σ acts as an integrator of the error vector $\tilde{\nu}$ under the condition that the saturation function is unsaturated (hence the name *conditional integrator*). In this case, the dynamics of σ in (8b) become

$$\dot{\sigma} = -\mathbf{G}\sigma + \mathbf{J}\mathbf{H}\left\{\mathbf{H}^{-1}\left[\tilde{\nu} + \mathbf{J}^{\top}\mathbf{G}\sigma\right]\right\} = \mathbf{J}\tilde{\nu}. \tag{12}$$

When the error $\tilde{\nu}$ is large, or reduces slowly, the signal σ can become large. This can possibly result in undesirable overshoot and integrator wind-up, which could destabilise the system. Due to the use of the saturation function in (8b) this is avoided, as it assures the signal σ is bounded. Using the Lyapunov function candidate $\mathcal{V}_{\sigma} = \frac{1}{2}\sigma^{\top}\mathbf{G}^{-1}\sigma$ we obtain

$$\begin{aligned} \dot{\mathcal{V}}_{\sigma} &= \sigma^{\top}\mathbf{G}^{-1}\dot{\sigma} = \sigma^{\top}\mathbf{G}^{-1}\left\{-\mathbf{G}\sigma + \mathbf{J}\mathbf{H}\mathrm{sat}(\mathbf{s})\right\} \\ &= -\sigma^{\top}\sigma + \sigma^{\top}\mathbf{G}^{-1}\mathbf{H}\mathbf{J}\mathrm{sat}(\mathbf{s}) \\ &\leq -\|\sigma\|^2 + \|\sigma\|\left\|\mathbf{G}^{-1}\mathbf{H}\right\|\|\mathbf{J}\|\|\mathrm{sat}(\mathbf{s})\| \\ &= -\|\sigma\|\left[\|\sigma\| - \left\|\mathbf{G}^{-1}\mathbf{H}\right\|\sqrt{n}\right], \end{aligned} \tag{13}$$

where n is the length of the vector $\mathrm{sat}(\mathbf{s})$ (in this case $n = 3$). From this it follows that $\dot{\mathcal{V}}_{\sigma} < 0$ for $\|\sigma\| > \left\|\mathbf{G}^{-1}\mathbf{H}\right\|\sqrt{n}$; chosing $\sigma(t_0) \leq \left\|\mathbf{G}^{-1}\mathbf{H}\right\|\sqrt{n}$ (the choice $\sigma(t_0) = \mathbf{0}$ always satisfies this), we have

$$\|\sigma(t)\| \leq \left\|\mathbf{G}^{-1}\mathbf{H}\right\|\sqrt{n} \qquad \forall \quad t \geq t_0, \tag{14a}$$
$$\|\hat{\epsilon}(t)\| \leq \|\mathbf{F}\|\sqrt{n} \qquad \forall \quad t \geq t_0, \tag{14b}$$

where the latter follows from following similar steps as in (13) for $\mathcal{V}_{\hat{\epsilon}} = \frac{1}{2}\hat{\epsilon}^{\top}\mathbf{G}^{-1}\hat{\epsilon}$, and using $\dot{\hat{\epsilon}} = \mathbf{K}_{\epsilon}^{-1}\dot{\sigma}$ from (10). Hence σ and $\hat{\epsilon}$ are bounded, resulting in integrator anti-windup. The bound on σ is directly related to the choice of the tuning matrices $\mathbf{G}$ and $\mathbf{H}$, while $\hat{\epsilon}$ has a bound influenced by the choice of $\mathbf{F}$.

IV. Error Dynamics

In order to gain theoretical insight into the effect of the tuning matrices $\{\mathbf{E},\, \mathbf{F},\, \mathbf{G},\, \mathbf{H}\}$, we discuss the error dynamics of the closed-loop system.

A. Position error dynamics

First we analyse the dynamics of the position error $\tilde{\eta}$ defined in (6). Using (1), (5) and $\mathbf{J}(\eta)\mathbf{J}^{\top}(\eta) = \mathrm{I}$ we have

$$\begin{aligned} \dot{\tilde{\eta}} &= \dot{\eta}_{\mathrm{d}} - \dot{\eta} = \dot{\eta}_{\mathrm{d}} - \mathbf{J}(\eta)\nu = \dot{\eta}_{\mathrm{d}} - \mathbf{J}(\eta)\left\{\nu_{\mathrm{c}} - \tilde{\nu}\right\} \\ &= \dot{\eta}_{\mathrm{d}} - \mathbf{J}(\eta)\left\{\mathbf{J}^{\top}(\eta)\left[\dot{\eta}_{\mathrm{d}} + \mathbf{E}\tilde{\eta}\right] - \tilde{\nu}\right\} = -\mathbf{E}\tilde{\eta} + \mathbf{J}(\eta)\tilde{\nu}. \end{aligned} \tag{15}$$

Using the auxiliary function $\mathcal{W}_{\tilde{\eta}} = \frac{1}{2}\tilde{\eta}^{\top}\tilde{\eta}$ we obtain

$$\begin{aligned} \dot{\mathcal{W}}_{\tilde{\eta}} &= \tilde{\eta}^{\top}\dot{\tilde{\eta}} = -\tilde{\eta}^{\top}\mathbf{E}\tilde{\eta} + \tilde{\eta}^{\top}\mathbf{J}(\eta)\tilde{\nu} \\ &\leq -\lambda_e\|\tilde{\eta}\|^2 + \|\tilde{\eta}\|\|\tilde{\nu}\|, \end{aligned} \tag{16}$$

where $\lambda_e > 0$ is the smallest eigenvalue of $\mathbf{E} \succ \mathbf{0}$. If $\tilde{\nu} = \mathbf{0}$, we have (see e.g. [7, Theorem 4.10])

$$\|\tilde{\eta}(t)\| \leq \|\tilde{\eta}(t_0)\|\, e^{-2\lambda_e(t-t_0)}, \tag{17}$$

which shows the error term vanishes at an exponential rate. Since λ_e depends on the choice of $\mathbf{E}$, the rate of convergence can be influenced by changing $\mathbf{E}$: the larger the smallest eigenvalue λ_e, the faster the position error will vanish.

B. Velocity error dynamics

The dynamics of the velocity error $\tilde{\nu}$ defined in (6) are discussed next. Combining (2) and (7) we obtain

$$\mathbf{M}\dot{\tilde{\nu}} + \mathbf{C}(\nu)\tilde{\nu} + \mathbf{D}(\nu)\tilde{\nu} = \mathbf{J}^{\top}(\eta)\epsilon + \bar{\tau}. \tag{18}$$

The undisturbed case: For $\epsilon = \mathbf{0}$ and $\bar{\tau} = 0$, this system is exponentially stable; the time-derivative of $\mathcal{V}_{\tilde{\nu}} = \frac{1}{2}\tilde{\nu}^{\top}\mathbf{M}\tilde{\nu}$ is

$$\dot{\mathcal{V}}_{\tilde{\nu}} = \tilde{\nu}^{\top}\mathbf{M}\dot{\tilde{\nu}} = -\tilde{\nu}^{\top}\mathbf{C}\tilde{\nu} - \tilde{\nu}^{\top}\mathbf{D}\tilde{\nu} = -\tilde{\nu}^{\top}\mathbf{D}\tilde{\nu} \leq 0, \tag{19}$$

where $\mathbf{C}(\nu)$ is skew-symmetric and $\mathbf{D}(\nu)$ is positive definite. Hence in this case $\tilde{\nu} \to \mathbf{0}$ is guaranteed, resulting in $\tilde{\eta} \to \mathbf{0}$ due to the exponential rate of convergence shown in (17).

The disturbed case: When there is an external disturbance ϵ (such as wind or ocean currents), we apply the conditional integrator $\bar{\tau}$ as given in (8), and analyse its effect on

$$\mathbf{M}\dot{\tilde{\nu}} = \mathbf{J}^{\top}(\eta)\epsilon + \bar{\tau} = \mathbf{J}^{\top}(\eta)\epsilon - \mathbf{F}\mathrm{sat}\left(\mathbf{s}\right). \tag{20}$$

Note that here we ignore the influence of the Coriolis and centripetal matrix $\mathbf{C}$ and damping matrix $\mathbf{D}$; as shown in [6] the stability analysis can be split; in this article it gives a better insight in the properties and influence of the conditional integrator (8).

When all elements of the error vector $\tilde{\nu}$ are large we have $\mathrm{sat}\left(\mathbf{s}\right) = \mathrm{sgn}\left(\tilde{\nu}\right)$, and the velocity error dynamics is given by

$$\mathbf{M}\dot{\tilde{\nu}} = \mathbf{J}^{\top}\epsilon - \mathbf{F}\,\mathrm{sgn}\left(\tilde{\nu}\right). \tag{21}$$

Using the Lyapunov function candidate $\mathcal{V}_{\tilde{\nu}} = \frac{1}{2}\tilde{\nu}^{\top}\mathbf{M}\tilde{\nu}$ gives

$$\begin{aligned}\dot{\mathcal{V}}_{\tilde{\nu}} &= \tilde{\nu}^{\top}\mathbf{M}\dot{\tilde{\nu}} = \tilde{\nu}^{\top}\left\{\mathbf{J}^{\top}\epsilon - \mathbf{F}\,\mathrm{sgn}\left(\tilde{\nu}\right)\right\} \\ &= \tilde{\nu}^{\top}\mathbf{J}^{\top}\epsilon - \sum_{i=1}^{3}\tilde{\nu}_i f_i\,\mathrm{sgn}\left(\tilde{\nu}_i\right) = \tilde{\nu}^{\top}\mathbf{J}^{\top}\epsilon - \left\|\mathbf{F}\tilde{\nu}\right\|_1 \\ &\leq \left\|\tilde{\nu}\right\|\left\|\mathbf{J}\right\|\left\|\epsilon\right\| - \left\|\mathbf{F}\tilde{\nu}\right\| \leq \left(\left\|\epsilon\right\| - \lambda_f\right)\left\|\tilde{\nu}\right\|,\end{aligned} \tag{22}$$

where $\lambda_f > 0$ denotes the smallest eigenvalue of $\mathbf{F}$; hence for $\mathbf{F} \succ \|\epsilon\|\,\mathrm{I}$ the conditional integrator adds to the convergence of $\tilde{\nu} \to \mathbf{0}$ as if it was a sliding-mode controller.

Using (10) we define the disturbance estimation error

$$\tilde{\epsilon} := \hat{\epsilon} - \epsilon = \mathbf{K}_{\epsilon}^{-1}\sigma - \epsilon. \tag{23}$$

It can be proven that the saturation function is guaranteed to become unsaturated. In this case—for ϵ constant and $\dot{\sigma}$ as given in (12)—the error vector $\tilde{\epsilon}$ has the dynamics

$$\dot{\tilde{\epsilon}} = \mathbf{K}_{\epsilon}^{-1}\dot{\sigma} = \mathbf{K}_{\epsilon}^{-1}\mathbf{J}\tilde{\nu} = \mathbf{F}\mathbf{G}\mathbf{H}^{-1}\mathbf{J}\tilde{\nu}. \tag{24}$$

The rate of convergence depends on the error term $\tilde{\nu}$; if $\tilde{\nu} \equiv \mathbf{0}$ the error signal $\tilde{\epsilon}$ stays constant, and it seems convergence of $\tilde{\epsilon} \to \mathbf{0}$ is not guaranteed. But the dynamics of $\tilde{\nu}$ in the unsaturated case are given by

$$\begin{aligned}\mathbf{M}\dot{\tilde{\nu}} &= \mathbf{J}^{\top}\epsilon - \mathbf{F}\left\{\mathbf{H}^{-1}\left[\tilde{\nu} + \mathbf{J}^{\top}\mathbf{G}\sigma\right]\right\} \\ &= \mathbf{J}^{\top}\epsilon - \mathbf{J}\mathbf{F}\mathbf{G}\mathbf{H}^{-1}\sigma - \mathbf{F}\mathbf{H}^{-1}\tilde{\nu} = -\mathbf{J}^{\top}\tilde{\epsilon} - \mathbf{F}\mathbf{H}^{-1}\tilde{\nu},\end{aligned} \tag{25}$$

revealing that $\dot{\tilde{\nu}} \neq \mathbf{0}$ for $\tilde{\nu} = \mathbf{0}$, $\tilde{\epsilon} \neq \mathbf{0}$, and hence we have $\tilde{\nu} \equiv \mathbf{0} \Leftrightarrow \tilde{\epsilon} \equiv \mathbf{0}$. Combining (24) and (25) gives

$$\dot{\mathbf{x}} = \begin{bmatrix}\dot{\tilde{\nu}} \\ \dot{\tilde{\epsilon}}\end{bmatrix} = \begin{bmatrix}-\mathbf{M}^{-1}\mathbf{F}\mathbf{H}^{-1} & -\mathbf{M}^{-1}\mathbf{J}^{\top} \\ \mathbf{F}\mathbf{G}\mathbf{H}^{-1}\mathbf{J} & \mathbf{0}\end{bmatrix}\begin{bmatrix}\tilde{\nu} \\ \tilde{\epsilon}\end{bmatrix} = \mathcal{G}\mathbf{x}. \tag{26}$$

We can apply a similarity transformation $\mathcal{H} = \mathcal{S}\mathcal{G}\mathcal{S}^{-1}$ where

$$\mathcal{H} = \begin{bmatrix}-\mathbf{L}^{\top}\mathbf{L} & -\mathbf{L}^{\top}\mathbf{G}\mathbf{L} \\ \mathrm{I} & \mathbf{0}\end{bmatrix} = \begin{bmatrix}\mathcal{A} & \mathcal{B} \\ \mathcal{C} & \mathcal{D}\end{bmatrix}, \tag{27}$$

$$\mathcal{S} = \begin{bmatrix}\mathbf{N}^{-1} & \mathbf{0} \\ \mathbf{0} & \mathbf{N}^{-1}\mathbf{J}^{\top}\mathbf{F}^{-1}\mathbf{G}^{-1}\mathbf{H}\end{bmatrix}, \tag{28}$$

where $\mathbf{L} := \mathbf{N}\left[\mathbf{F}\mathbf{H}^{-1}\right]^{\frac{1}{2}}$ and $\mathbf{N}$ is the unique square root of the inverse of the symmetric positive definite matrix $\mathbf{M}$, such that $\mathbf{M}^{-1} = \mathbf{N}^2$. Since similar matrices have the same eigenvalues ([8, Corollary 1.3.4]), we can analyse the eigenvalues of matrix $\mathcal{H}$; since $\mathcal{C} = \mathrm{I}$ (and hence commutes with all matrices) they can be found by solving ([9])

$$\begin{aligned}&\det([\lambda\mathrm{I} - \mathcal{A}]\left[\lambda\mathrm{I} - \mathcal{D}\right] - \mathcal{B}\mathcal{C}) \\ &= \det(\lambda^2\mathrm{I} + \lambda\mathbf{L}^{\top}\mathbf{L} + \mathbf{L}^{\top}\mathbf{G}\mathbf{L}) = \mathbf{0}.\end{aligned} \tag{29}$$

We note that this system resembles an unforced mass-spring-damper system (see e.g. [10, Chapter 14]) with mass matrix $\mathcal{M} = \mathrm{I}$, damping matrix $\mathcal{D} = \mathbf{L}^{\top}\mathbf{L}$, and stiffness matrix $\mathcal{K} = \mathbf{L}^{\top}\mathbf{G}\mathbf{L}$ given by

$$\mathcal{M}\frac{d^2\mathbf{p}}{dt^2} + \mathcal{D}\frac{d\mathbf{p}}{dt} + \mathcal{K}\mathbf{p} = \mathbf{0}, \tag{30}$$

for position $\mathbf{p}$, or equivalently it resembles an unforces resistor-capacitor-inductor system (RCL system) (see e.g. [10, Chapter 31]) with inductance matrix $\mathcal{L} = \mathrm{I}$, resistance matrix $\mathcal{R} = \mathbf{L}^{\top}\mathbf{L}$, and capacitance matrix $\mathcal{C} = \left[\mathbf{L}^{\top}\mathbf{G}\mathbf{L}\right]^{-1}$ given by

$$\mathcal{L}\frac{d^2\mathbf{q}}{dt^2} + \mathcal{R}\frac{d\mathbf{q}}{dt} + \mathcal{C}^{-1}\mathbf{q} = \mathbf{0}, \tag{31}$$

for charge $\mathbf{q}$. Using these analogues, we know that increasing the tuning matrix $\mathbf{G}$ increases the stiffness matrix $\mathcal{K}$/decreases the capacitance matrix $\mathcal{C}$, resulting in higher natural frequencies (eigenvalues).

V. Controller Tuning

The controller has four distinct tuning parameters: $\{\mathbf{E}, \mathbf{F}, \mathbf{G}, \mathbf{H}\}$. The effect of changing one of these parameters has a clear effect on the performance of the system. Tuning the controller parameters is a trade-off between different desired effects, which in this case are: convergence towards the trajectory, reducing the velocity error $\tilde{\nu}$ to zero, and obtaining correct and reliable estimates of the disturbance ϵ.

For showing the effect of tuning, we consider a curved trajectory as shown by the dotted, black line in Figure 1. An ocean current is modelled as a constant force

$$\epsilon = [0.2;\ -0.2;\ 0.0], \tag{32}$$

and its direction is indicated in the figure.

The tuning parameters are diagonal matrices, chosen as

$$\begin{aligned}\mathbf{E} &= \mathrm{diag}\left(0.05;\ 0.05;\ 0.50\right) \\ \mathbf{F} &= \mathrm{diag}\left(1.0;\ 1.0;\ 5.0\right) \\ \mathbf{G} &= \mathrm{diag}\left(2.0;\ 2.0;\ 12.5\right) \\ \mathbf{H} &= \mathrm{diag}\left(0.1;\ 0.1;\ 0.5\right)\end{aligned} \tag{33}$$

which will be referred to as the *normal* values. For showing the effect of changing the parameters, we have used *small* values (which are half the normal values) and *large* values (which are twice the normal values). The effect of using these three distinct values will be discussed per parameter next.

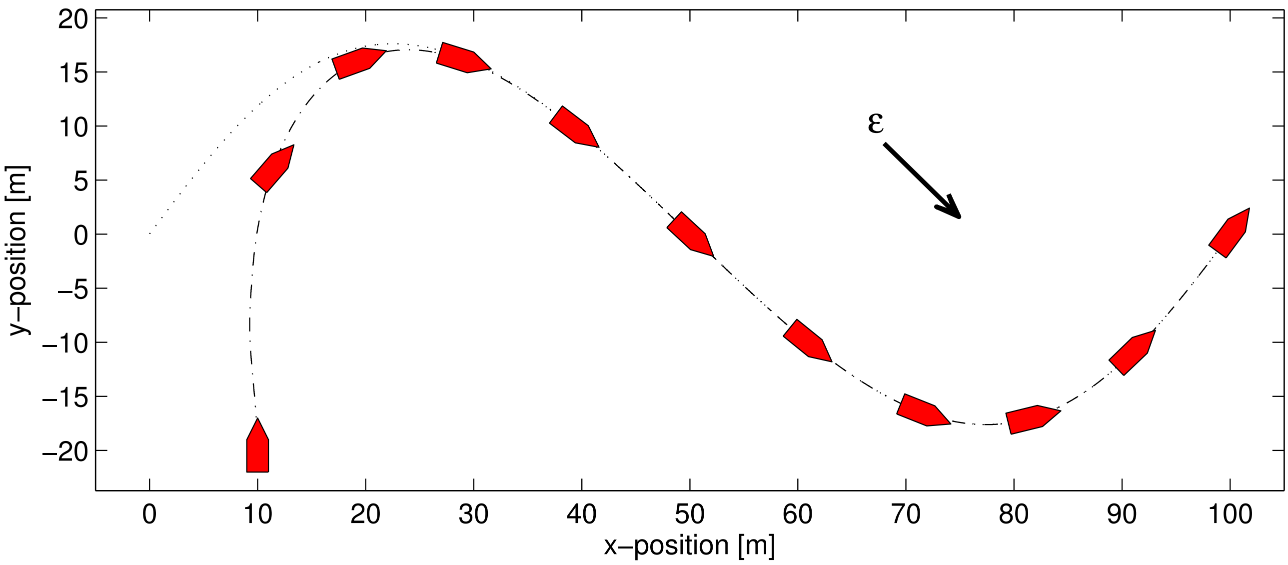

Fig. 1. Target tracking in the presence of constant external disturbances

A. *Effect of changing* $\mathbf{E}$

Changing the value of $\mathbf{E}$ has a direct effect on the rate of convergence towards the desired trajectory, as can be seen in Figure 2. As $\mathbf{E}$ is chosen larger, the vessel will converge to the path faster, which is preferrable. This effect can be traced back to the dynamics of position error $\tilde{\eta}$ given in (15).

The negative effect of increasing $\mathbf{E}$ can be seen in the plots for the velocity error $\tilde{\nu}$ in Figure 3. Increasing $\mathbf{E}$ increases the magnitudes of the desired velocity terms (due to the definition of ν_{c} in (5)), which increases the time it takes for the velocity errors to converge to zero.

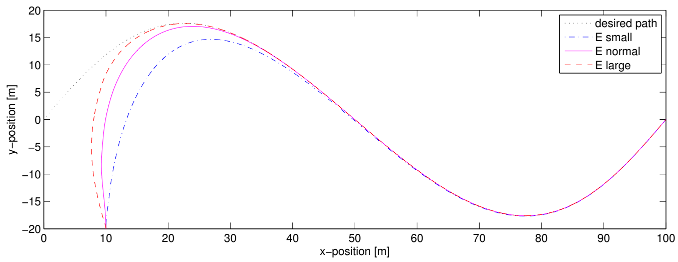

Fig. 2. Effect of changing $\mathbf{E}$ on the convergence towards the trajectory

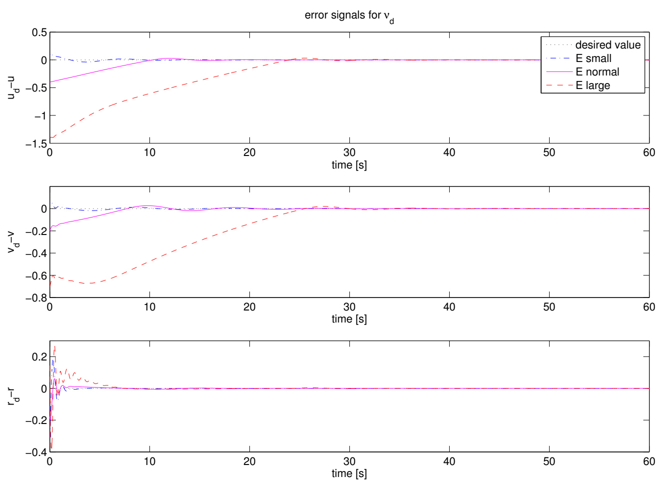

Fig. 3. Effect of changing $\mathbf{E}$ on the velocity error $\tilde{\nu}$

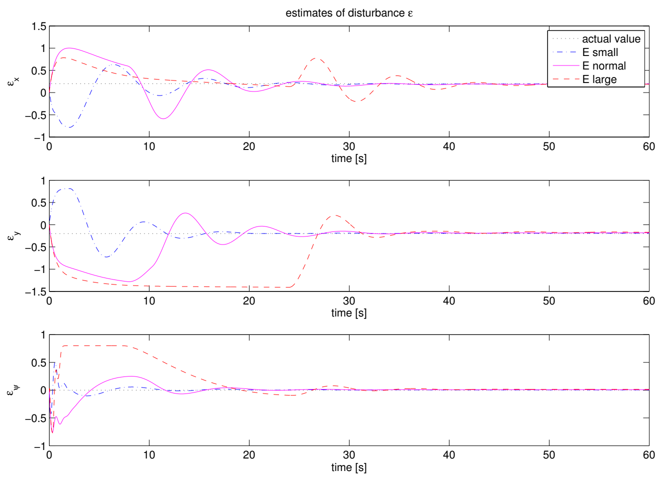

Fig. 4. Effect of changing $\mathbf{E}$ on the estimation of disturbance ϵ

Furthermore the estimation of the disturbance ϵ becomes slower when $\mathbf{E}$ gets larger, as can be seen in Figure 4. This is since convergence of $\tilde{\epsilon} \rightarrow \mathbf{0}$ is only guaranteed when the velocity error $\tilde{\nu}$ is small (such that the saturation function in (8) is unsaturated), and hence the slower convergence of $\tilde{\nu}$ results in a later start of converging of $\tilde{\epsilon}$. The boundedness of $\tilde{\epsilon}$ predicted in (14b) shows in the lower subplots of Figure 4 for the case where $\mathbf{E}$ is large.

B. Effect of changing *F*

Changing the value of $\mathbf{F}$ has a negligible effect on the convergence towards the trajectory.

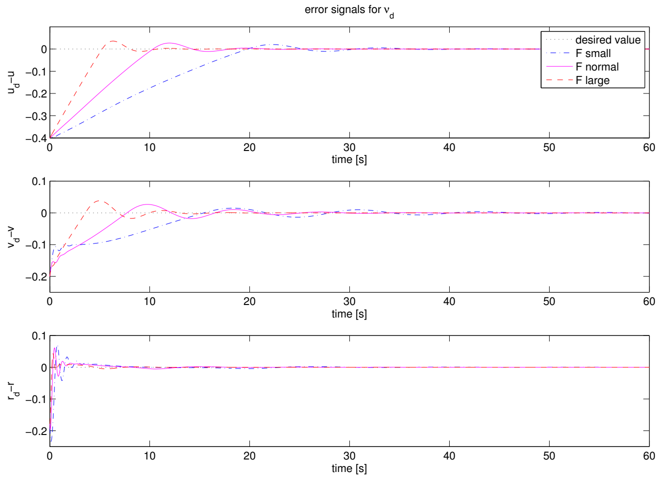

Fig. 5. Effect of changing $\mathbf{F}$ on the velocity error $\tilde{\nu}$

The velocity error $\tilde{\nu}$ converges faster as $\mathbf{F}$ gets larger, but at the cost of slightly larger overshoot, as shown in Figure 5. Initially the sliding-mode control behaviour shown in (21) is clearly present as shown by the initial fast convergence at a fixed rate; doubling the values of $\mathbf{F}$ results in halving the rise time. Also in the unsaturated case increasing $\mathbf{F}$ results in faster convergence of $\tilde{\nu}$, as is expected from (25).

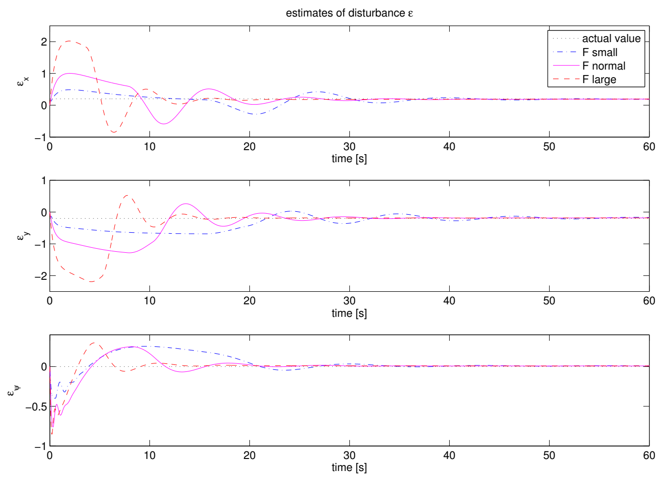

Fig. 6. Effect of changing $\mathbf{F}$ on the estimation of disturbance ϵ

The disadvantage of increasing $\mathbf{F}$ can be found in the disturbance estimation. Although resulting in faster convergence, Figure 6 shows that increasing $\mathbf{F}$ increases the magnitude of the signal, which could make it unsuitable for feed-back due to the unrealistically large values. The effect of $\mathbf{F}$ on the bound on $\hat{\epsilon}$ is shown in (14b).

C. Effect of changing *G*

Changing the value of $\mathbf{G}$ has a negligible effect on the convergence towards the trajectory. Increasing $\mathbf{G}$ will make the velocity errors converge slightly faster, as can be seen in Figure 7.

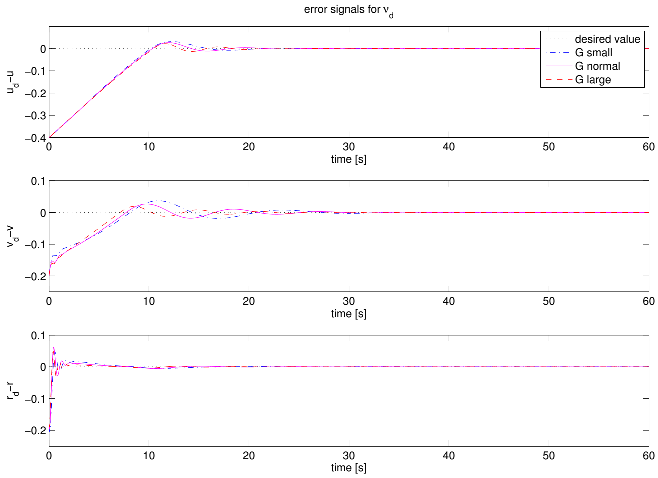

Fig. 7. Effect of changing $\mathbf{G}$ on the velocity error $\tilde{\nu}$

Increasing $\mathbf{G}$ also results in faster convergence of the disturbance estimate $\hat{\epsilon}$, as shown in Figure 8. The disadvantage of increasing $\mathbf{G}$ is in the faster response in $\hat{\epsilon}$ shown as a higher frequency oscillation in Figure 8, due to the increase in the natural frequency as discussed in Section IV. This might lead to instabilities when using the estimates in closed-loop due to having a more 'nervous' system.

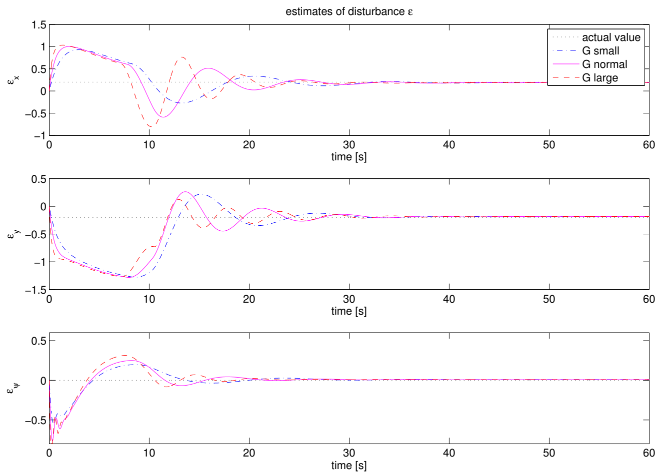

Fig. 8. Effect of changing $\mathbf{G}$ on the estimation of disturbance ϵ

D. Effect of changing *H*

Changing the value of $\mathbf{H}$ has a negligible effect on the convergence towards the trajectory. Increasing $\mathbf{H}$ results in slower convergence of the velocity error $\tilde{\nu}$ with larger overshoot, as shown in Figure 9, accounted for by the reduction of the gain $\mathbf{FH}^{-1}$ in (25).

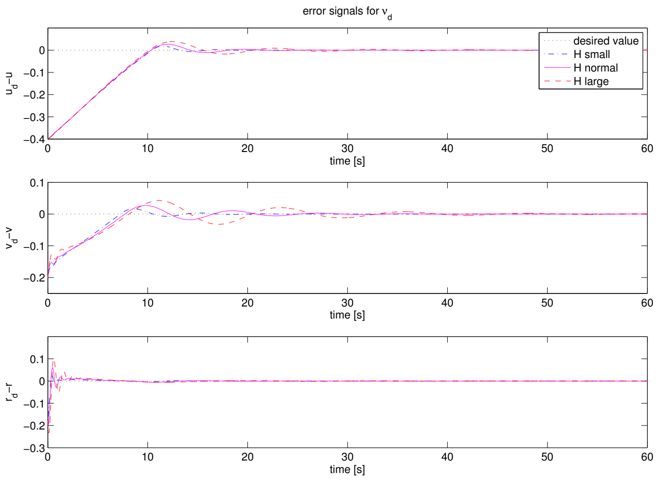

Fig. 9. Effect of changing $\mathbf{H}$ on the velocity error $\tilde{\nu}$

For the disturbance estimation, increasing $\mathbf{H}$ results in slower convergence, but also in a lower frequency oscillation of the signal, due to the decrease of $\mathbf{L} = \mathbf{N}\left[\mathbf{FH}^{-1}\right]^{\frac{1}{2}}$ in (27) and (29), thereby reducing the eigenfrequency of the system. This results in a 'calmer' closed-loop system when using $\hat{\epsilon}$ for feed-back.

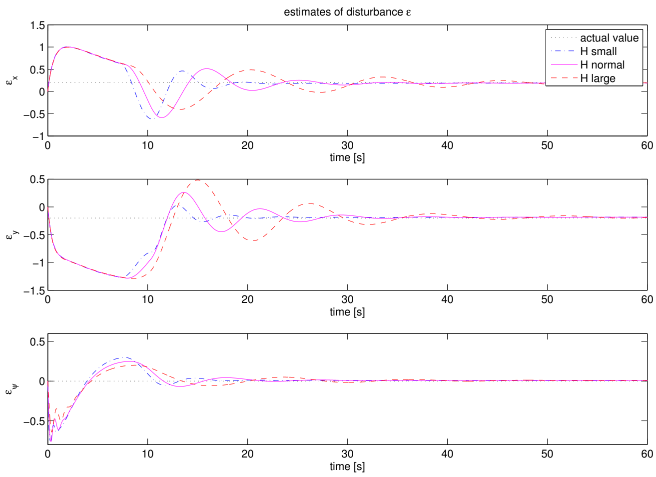

Fig. 10. Effect of changing $\mathbf{H}$ on the estimation of disturbance ϵ

E. Summary of the tuning rules

Based on the discussion above, we summarise the tuning rules with the focus on five desirable properties:

1) *Fast convergence towards the desired position* η_d
2) *Fast convergence towards the desired velocity* ν_d
3) *Fast convergence of the disturbance estimation* $\hat{\epsilon}$
4) *Small bound on the disturbance estimation* $\hat{\epsilon}$
5) *Low eigenfrequencies for the disturbance estimation*

In the table below these five properties are denoted by their respective number on the left, while the effect of the tuning matrix given at the top is marked as follows:

- + increasing has a positive effect on the property
- o increasing has a negligible effect on the property
- - increasing has a negative effect on the property

This results in the following table of tuning rules:

TUNING RULES	**E**	**F**	**G**	**H**
1) *Position error*	+	o	o	o
2) *Velocity error*	-	+	+	-
3) *Estimation error*	-	+	o	-
4) *Estimation bound*	o	-	o	o
5) *Eigenfrequency*	o	-	-	+

Reading this table from the perspective of improving a certain property, one can read what one should do with a tuning matrix to obtain this goal: $+$ means increasing the gain, while $-$ means decreasing it.

VI. Conclusions

We have proposed a control strategy to obtain guaranteed convergence and stability for target tracking of surface vessels in the presence of unknown constant disturbances, which is proven analytically in previous work. Here we show that the controller is easy to tune, by discussing the effect of the four different tuning matrices on the system both graphically and theoretically. This article can be considered as a guideline for tuning the proposed controller.

VII. Acknowledgements

This research is supported by the European Union, through the Marie Curie Research Training Network FREE$_{\text{sub}}$NET (FP6, MRTN-CT-2006-036186), and the Norwegian Research Council through (NFR 189839/V11).

References

[1] M. Burger, A. Pavlov, and K. Y. Pettersen, "Conditional integrators for path following and formation control of marine vessels under constant disturbances," in *Manoeuvring and Control of Marine Craft*. Guarujá, Brazil: IFAC, Sep. 2009, pp. 179–184.

[2] ——, "Curved trajectory tracking for surface vessels under constant external disturbances," in *7th Symposium on Intelligent Autonomous Vehicles*. Lecce, Italy: IFAC, Sep. 2010, submitted.

[3] S. Seshagiri and H. K. Khalil, "Robust output feedback regulation of minimum-phase nonlinear systems using conditional integrators," *Automatica*, vol. 41, no. 1, pp. 43–54, Jan. 2005.

[4] A. Singh and H. K. Khalil, "Regulation of nonlinear systems using conditional integrators," *International Journal of Robust and Nonlinear Control*, vol. 15, no. 8, pp. 339–362, Jul. 2005.

[5] T. I. Fossen, *Marine Control Systems - Guidance, Navigation and Control of Ships, Rigs and Underwater Vehicles*, 3rd ed. Marine Cybernetics, 2002.

[6] M. Burger, A. Pavlov, and K. Y. Pettersen, "Curved trajectory tracking for surface vessel formations," in *Conference on Decision and Control*. Atlanta, USA: IEEE, Dec. 2010, submitted.

[7] H. K. Khalil, *Nonlinear Systems*, 3rd ed. Prentice Hall, 2002.

[8] R. Horn and C. Johnson, *Matrix Analysis*. Cambridge University Press, 1990.

[9] F. Zhang, *The Schur Complement and Its Applications*, ser. Numerical Methods and Algorithms. Springer, 2005, vol. 4.

[10] P. Tipler, *Physics for Scientists and Engineers*, 4th ed. W.H. Freeman, 1998.